Inherent Limitations in Data-Aided Time Synchronization of Continuous Phase-Modulation Signals Over Time-Selective Fading Channels

Ron Dabora, Jason Goldberg, *Senior Member, IEEE*, and Hagit Messer, *Fellow, IEEE*

***Abstract*—Time synchronization of continuous phase modulation (CPM) signals over time selective, Rayleigh fading channels is considered. The Cramér–Rao lower bound (CRLB) for this problem is studied for data-aided (DA) synchronization (i.e., known symbol sequence transmission) over a time-selective Rayleigh fading (i.e., Gaussian multiplicative noise) channel. Exact expressions for the bound are derived as well as simplified, approximate forms that enable derivation of a number of properties that describe the bound's dependence on key parameters such as signal-to-noise ratio (SNR), channel correlation, sampling rate, sequence length, and sequence choice. Comparison with the well-known slow fading (i.e., constant) channel bound is emphasized. Further simplifications are obtained for the special case of minimum phase keying (MSK), wherein it is shown how the bound may be used as a *sequence design tool* to optimize synchronization performance.**

***Index Terms*—Continuous phase modulation, Cramér–Rao bound, fading channels, minimum shift keying, synchronization, timing.**

I. Introduction

CONTINUOUS phase modulation (CPM) is an important class of digital modulation that combines good spectral efficiency with the desirable property of constant signal modulus. This latter characteristic enables use of highly efficient, nonlinear power amplification in transmission and provides inherent robustness to amplitude fading in reception, e.g., [1]. It is well known that like all other digital modulation schemes, application of CPM requires synchronization of the time reference of the receiver to that of the received signal. Due to the popularity of CPM, considerable effort has been directed toward the problem of time synchronization for such signals, e.g., [2]–[4]. Nevertheless, most work on this subject has concentrated on the additive white Gaussian noise (AWGN) channel with relatively little research directly addressing CPM time synchronization over *fast fading* (i.e., time-varying) channels (see [5] for an exception).

Manuscript received August 14, 2000; revised January 15, 2002. This work was supported in part by the Israeli Science Foundation founded by the Academy of Sciences and Humanities. The associate editor coordinating the review of this paper and approving it for publication was Dr. Inbar Fijalkow.

R. Dabora was with the Department of Electrical Engineering-Systems, Tel Aviv University, Tel Aviv, Israel. He is now with the Algorithms Development Group, Millimetrix Broadband Networks, Tel Aviv, Israel.

J. Goldberg is with the Department of Electrical Engineering—Systems, Tel Aviv University, Tel Aviv, Israel, and also with the Cellular Communications Division, Intel, Petach Tikva, Israel (e-mail: jason@eng.tau.ac.il).

H. Messer is with the Department of Electrical Engineering—Systems, Tel Aviv University, Tel Aviv, Israel (e-mail: messer@eng.tau.ac.il).

Publisher Item Identifier S 1053-587X(02)04397-0.

In addition, while the general problem of time synchronization over fast fading channels has been considered in the literature, e.g., [2], [6]–[8], some of this work either neglects the statistical nature of the fading or imposes additional signal assumptions. For example, in [2], a high SNR approximation removes the influence of the fading statistics from the problem, and in [6], the channel is simply treated as deterministic time varying, whereas in [8], a low SNR type "low energy coherence" assumption is used. Time synchronization for linear modulation types is considered in [9] and [10], where a cyclostationary approach is used, and [11], which uses a delay-and-multiply method. In [12], a cyclostationary approach is applied to blind synchronization of MSK signals over time selective fading channels.

A study of the inherent limitations in the estimation of fading parameters (Doppler shift, Doppler rate, and LOS component strength) was carried out in [13] and [14] under the assumption of *perfect time synchronization*. However, an analysis of the *inherent limitations* in time synchronization accuracy for fast fading channels does not appear to have been treated in detail in the literature for any type of signal. Note that in [10], a CRLB is derived for blind time-delay estimation for *linear* modulation by calculating the covariance of the transmitted signal (which is restricted to be real) and then imposing Gaussianity on the received signal. In addition, [10] does not contain an analysis of the bound and is focused mainly on estimation. Finally, a general study of the CRLB for parameters describing the deterministic phase component of a constant modulus signal subject to real Gaussian multiplicative noise can be found in [15].

This paper seeks to characterize the inherent performance limitations associated with CPM time synchronization over fading channels via a Cramér–Rao lower bound (CRLB) analysis. In particular, time-selective fading is assumed, wherein the channel manifests itself as zero mean complex Gaussian "multiplicative noise," giving rise to well-known Rayleigh-type amplitude fading, e.g., [1]. In addition, attention is focused on *data-aided (DA)* synchronization, wherein the transmitted symbol sequence is known *a priori*. Such a scenario may arise, for example, in communications systems that use some sort of known pilot transmission to synchronize the receiver to the transmitter. Another possible application is burst transmission where a known preamble is transmitted every burst (or every few bursts) to allow correction of the receiver's reference clock. Moreover, the DA CRLB for delay estimation can also be applied to decision-directed (DD) estimation, where it constitutes a relatively looser lower bound since DD synchronization is prone to bursty type of error events that typically cause a larger error variance. General CPM is considered along with the special case of minimum shift keying (MSK) e.g., [1].

The paper is structured as follows. Section II reviews CPM and MSK, compares two fast-fading channel correlation models, and specifies the overall model for the received data. The problem to be solved is formulated, and the well-known slow fading channel model is briefly reviewed. In Section III, explicit, exact, and approximate expressions for the CRLB are presented for both the slow fading and fast fading bounds for general CPM as well as MSK. Section IV derives a variety of properties that describe the bound's dependence on a number of key parameters such as SNR, channel correlation, and sequence length. Section V presents numerical examples to illustrate the results. Section VI introduces an application of the bound for synchronization sequence design. Last, Section VII summarizes the work.

II. Modeling and Problem Formulation

Begin by considering a general, discrete-time complex baseband signal received over a time-selective fading channel and sampled at sampling interval T_s

$$y[k] = f[k]s[k, \tau] + n[k] \tag{1}$$

where $f[k]$, $s[k, \tau] = s(kT_s - \tau)$, and $n[k]$ are the baseband equivalent time-varying channel, transmitted signal, and additive noise components, respectively. The channel component will be assumed to be a realization of a zero mean, stationary circular, complex Gaussian random process $f[k] \sim \mathcal{CN}(0, \sigma_f^2)$ of correlation sequence $R_f[n] \triangleq E\{f[k]f^*[k-n]\}$ with $\sigma_f^2 = R_f[0]$. Gaussianity of the channel gives rise to the well-known Rayleigh distributed amplitude fading. The received signal component $s[k, \tau]$ is simply the transmitted signal subject to a delay τ. The additive noise is assumed to be a realization of a sequence of independent, identically distributed (IID) zero mean, circular, complex Gaussian random variables $n[k] \sim \mathcal{CN}(0, \sigma_n^2)$.

Before formulating the exact problem to be solved, CPM is briefly reviewed, and distinct parametric forms of the channel correlation sequence are presented.

A. Continuous Phase Modulation

The continuous time complex envelope of a CPM waveform may be written as, e.g., [16]

$$s(t) = \sqrt{\frac{E_s}{T_{sym}}}\, e^{j[\varphi(t, \boldsymbol{\eta}) + \varphi_0]} \tag{2}$$

where

E_s	symbol energy;
T_{sym}	symbol duration;
$\varphi(t, \boldsymbol{\eta})$	information bearing phase;
φ_0	arbitrary phase shift (which can be incorporated into the fading process and is thus taken to be zero).

The information-bearing phase component can be expressed as

$$\varphi(t, \boldsymbol{\eta}) = 2\pi h \int_{-\infty}^{t} \sum_{i=-\infty}^{\infty} \eta_i g(\zeta - iT_{sym})\, d\zeta; \qquad \forall\, t \tag{3}$$

where $\boldsymbol{\eta} = [\ldots, \eta_{-2}, \eta_{-1}, \eta_0, \eta_1, \ldots]^T$ is an infinitely long sequence of M-ary data symbols, each taking one of the values

$$\eta_i = \pm 1, \pm 2, \ldots, \pm(M-1); \qquad i = 0, \pm 1, \pm 2, \ldots \tag{4}$$

where M is assumed even. The variable h and the function $g(t)$ are referred to as the modulation index and the frequency pulse shape, respectively.

MSK signaling is a special case of CPM formed by setting $h = 1/2$ and $M = 2$ while employing the "1REC" frequency pulse shape

$$g(t) = \begin{cases} 0, & t < 0,\ t > T_{sym} \\ \dfrac{1}{2T_{sym}}, & 0 \le t \le T_{sym}. \end{cases} \tag{5}$$

It is noted that MSK may be viewed as a form of binary continuous-phase frequency shift keying (CPFSK), where one of two frequencies F_L and F_H [such that $F_H - F_L = 1/(2T_b)$] is transmitted every T_b seconds. MSK can also be represented in terms of linear modulation, e.g., [17]

$$\begin{aligned} s(t) &= \sqrt{\frac{E_b}{T_b}} \left\{ m_I(t) \cos\left(\frac{\pi t}{2T_b}\right) - j m_Q(t) \sin\left(\frac{\pi t}{2T_b}\right) \right\} \\ m_I(t) &= \sum_{k=1,3,5,\ldots} u_k p(t - 2kT_b + T_b) \\ m_Q(t) &= \sum_{k=2,4,6,\ldots} u_k p(t - 2kT_b) \\ p(t) &= \begin{cases} 1, & t \in [0, 2T_b) \\ 0, & t \notin [0, 2T_b) \end{cases} \end{aligned} \tag{6}$$

where T_b and E_b are the bit period and bit energy, respectively, which, for MSK, satisfy $T_b = T_{sym}$ and $E_b = E_s$. As can be seen, $m_I(t)$ and $m_Q(t)$ are generated from the original bit stream by taking only the odd bits for $m_I(t)$ and multiplying them with a rectangular pulse train with pulse length of $2T_b$. The same is done for $m_Q(t)$ with the even bits; however, $m_Q(t)$ is also staggered by T_b with respect to $m_I(t)$. The relation between the two representations in (3) and (6) is given by $\eta_i = u_i u_{i-1}$.

B. Fading Modeling and Fading Statistics

The Rayleigh fading model is commonly employed in so-called nonline-of-sight (NLOS) propagation conditions, where multiple signal components arrive at the receiver *indirectly* via scattering, diffraction, and reflection effects, e.g., [1]. If the RMS variation in the arrival time of these channel components is less than a symbol period, then the effect of the channel can be approximated as purely *multiplicative*, giving rise to the model in (1).

Motion of the receiver, the transmitter, or objects present in the propagation environment all contribute to the time-varying nature of the channel. Under the zero mean, stationary, circular complex Gaussian model of (1), the time-varying nature of the channel is completely characterized by its correlation sequence or, equivalently, its Doppler spectrum. A commonly used model for land-mobile communications scenarios with isotropic scattering and horizontal propagation is the "U-shaped" Jakes Doppler spectrum [18]

$$S_f^J(\omega) = \begin{cases} \sigma_f^2 \dfrac{1}{\omega_m/2} \dfrac{1}{\sqrt{1 - \left(\frac{\omega}{\omega_m}\right)^2}}, & |\omega| \le \omega_m \\ 0, & \text{otherwise} \end{cases} \tag{7}$$

where ω_m is the maximum Doppler shift in radians per second, which, for the above model, also corresponds to the Doppler bandwidth B_D^J. The associated correlation sequence is

$$R_f^J(m) = \sigma_f^2 J_0(\omega_m m T_s) \tag{8}$$

where $J_0(\cdot)$ is the zero-order Bessel function of the first kind. Though common, this representation of the fading process correlation was not found to enable derivation of CRLB expressions that give analytical insight into the CPM time synchronization problem.[1] Thus, for the sake of analytical tractability, the channel will be modeled as an autoregressive process (e.g., [14]) of order one (AR1)[2]

$$f[k] = \alpha f[k-1] + \sqrt{1-\alpha^2} w[k], \quad w[k] \sim \mathcal{CN}(0, \sigma_f^2) \tag{9}$$

where $w[k]$ is IID.

Although the results obtained with this simplified model are not numerically identical to the results obtained with the Jakes model, the *analytical* insight obtained under the AR1 model also applies to the Jakes model (see Sections V and VI). Under this model, the channel correlation function may be written as

$$R_f^{AR}[m] = \sigma_f^2 \beta^{T_s|m|} = \sigma_f^2 \alpha^{|m|} \tag{10}$$

where β is the correlation parameter of the continuous time fading process, and $\alpha = \beta^{T_s}$ can be viewed as an "effective correlation parameter" induced by the channel as well as the sampling rate. Thus, for $\alpha = 0$, we model the channel as an uncorrelated fading process, and with $\alpha = 1$, we model the channel as a realization of a single random variable. The corresponding Doppler spectrum is given by

$$S_f^{AR}(\omega) = \sigma_f^2 \frac{-2\ln\beta}{\omega^2 + \ln^2\beta} \tag{11}$$

where, for this spectrum, the Doppler bandwidth B_D^{AR} will be defined as the 3-dB bandwidth of the spectrum, which is easily shown to be

$$B_D^{AR} = -\frac{1}{2\pi}\ln\beta = -\frac{1}{2\pi T_s}\ln(\alpha)\ [\text{Hz}]. \tag{12}$$

Note that for both the Jakes and AR1 correlation models, the amplitude of the fading process is Rayleigh distributed, and the phase is uniformly distributed over $[-\pi, \pi)$. To aid in visualizing the differences between the two models, Fig. 1 presents their respective temporal correlation functions. The graphs were drawn for normalized time-Doppler product of $T_b B_d = 0.1$ and $\sigma_f^2 = 1$. The value of α that corresponds to this time-doppler product, when $T_s = T_b$, is $\alpha = e^{-2\pi T_s B_d} = 0.53$. As can be seen from the figure, the correlation produced by the AR1 model lacks the oscillations present in the Jakes model; therefore, there is no strong peak at ω_m, and the spectrum decays more slowly with frequency.

[1]While relatively simple, low-order Taylor series approximations of (8) were found to be of poor accuracy.

[2]Note that at least for frequency estimation, both [14] and [19] claim that the actual shape of the Doppler spectrum has no noticeable effect on performance.

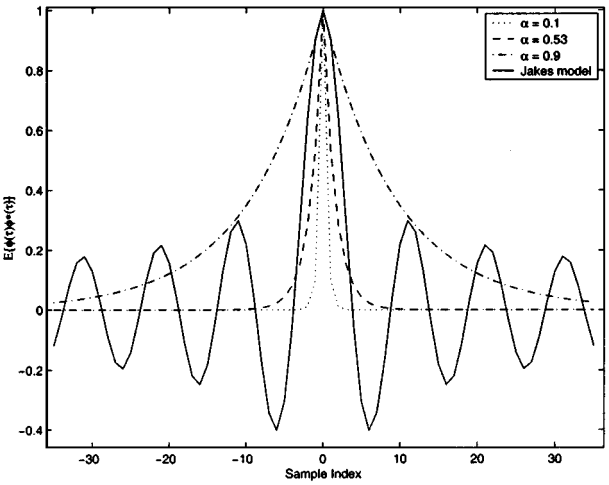

Fig. 1. Temporal correlation of the fading process for $B_d T_b = 0.1$ for the Jakes model and for the AR1 fading correlation model.

C. Statistics of the Received Signal

Assume an observation interval of N samples giving rise to $\{y[i]\}_{i=0}^{N-1}$, which, from (1), may be written in matrix form as

$$\begin{aligned} &\mathbf{y} = \mathbf{S}\mathbf{f} + \mathbf{n} \\ &\mathbf{y} = [y[0], \ldots, y[N-1]]^T \\ &\mathbf{f} = [f[0], \ldots, f[N-1]]]^T \\ &\mathbf{S} = \text{diag}[\mathbf{s}], \\ &\mathbf{s} = [s[0, \tau], s[1, \tau], \ldots, s[N-1, \tau]]^T \end{aligned} \tag{13}$$

with $[\cdot]^T$ denoting the transpose operation, and diag$[\cdot]$ denoting a diagonal matrix of specified diagonal elements. Note that the diagonal elements of $\mathbf{S}$ are the sampled modulated sequence, which depends on the K transmitted symbols $\boldsymbol{\eta} = [\eta_0, \eta_1, \ldots, \eta_{K-1}]^T$ and on the modulation scheme. For MSK, it is convenient to define a *bit vector* $\mathbf{u} = [u_0, u_1, \ldots, u_{K-1}]^T$. We now calculate the statistics of the received signal.

Since the transmitted signal $\mathbf{s}$ is known, $\mathbf{y}$ of (13) is a sum of two zero-mean complex Gaussian random vectors, and hence, $\mathbf{y}$ is also a zero-mean complex Gaussian random vector with correlation matrix given by

$$E\{\mathbf{y}\mathbf{y}^H\} = \mathbf{R}_\mathbf{y} = \mathbf{S}\mathbf{R}_\mathbf{f}\mathbf{S}^H + \sigma_n^2\mathbf{I}, \quad \mathbf{R}_\mathbf{f} = E\{\mathbf{f}\mathbf{f}^H\} \tag{14}$$

where

$[\cdot]^H$ conjugate transposition;
$\mathbf{I}$ $N \times N$ identity matrix,
$\mathbf{R}_\mathbf{f}$ fading channel correlation matrix.

The specific fading channel correlation matrix depends on the fading statistics. For the AR1 model, use of (10) yields the following correlation matrix:

$$\mathbf{R}_\mathbf{f} = \sigma_f^2 \begin{bmatrix} 1 & \alpha & \alpha^2 & \cdots & \alpha^{N-1} \\ \alpha & 1 & \alpha & \cdots & \alpha^{N-2} \\ \alpha^2 & \alpha & 1 & \cdots & \alpha^{N-3} \\ \vdots & \vdots & \vdots & \ddots & \vdots \\ \alpha^{N-1} & \alpha^{N-2} & \alpha^{N-3} & \cdots & 1 \end{bmatrix} \tag{15}$$

whose inverse will be important in the sequel, e.g., [14]

$$\mathbf{R}_{\mathbf{f}}^{-1} = \frac{1}{\sigma_f^2(1-\alpha^2)} \begin{bmatrix} 1 & -\alpha & 0 & \cdots & 0 \\ -\alpha & 1+\alpha^2 & -\alpha & \cdots & 0 \\ 0 & -\alpha & 1+\alpha^2 & \cdots & 0 \\ \vdots & \vdots & \vdots & \ddots & \vdots \\ 0 & 0 & 0 & \cdots & 1 \end{bmatrix}. \quad (16)$$

It should be noted that such a model was used for the spatial correlation in [20] for the case of angle estimation with an array of sensors where the data is corrupted by *spatial* multiplicative noise.[3]

The probability density function (PDF) for the received signal can now be written as

$$f(\mathbf{y};\boldsymbol{\theta}) = \frac{1}{\pi^N |\mathbf{R}_{\mathbf{y}}|} e^{-\mathbf{y}^H \mathbf{R}_{\mathbf{y}}^{-1}\mathbf{y}} \quad \boldsymbol{\theta} = [\tau,\, \sigma_f^2,\, \sigma_n^2,\, \alpha]^T \quad (17)$$

where $|\cdot|$ denotes the determinant of a matrix.

Before formally stating the problem to be solved, it should be noted that since it is impossible to distinguish between the fading channel power σ_f^2 and the signal power E_s/T_{sym}, we will use σ_f^2 to represent their product (i.e., the signal power is normalized to one) such that SNR is defined as $\rho = \sigma_f^2/\sigma_n^2$.

D. Estimation Problem

The estimation problem can now be formulated as follows: Given a received signal $\mathbf{y}$ with PDF (17), which is parameterized by an unknown parameter vector $\boldsymbol{\theta}$, estimate the time delay τ. In this problem, τ is the parameter of interest, and the three remaining parameters are *nuisance* parameters.

In the sequel, the results for the fast fading channel will be compared with those of the *slow fading* case described by, e.g., [21]

$$\mathbf{y}^{\mathrm{sf}} = f\mathbf{s} + \mathbf{n}, \quad f \sim \mathcal{CN}(0,\, \sigma_f^2) \quad (18)$$

with unknown parameter vector $\boldsymbol{\theta}^{\mathrm{sf}} = [\tau,\, \sigma_f^2,\, \sigma_n^2]^T$ and correlation matrix $\mathbf{R}_{\mathbf{y}}^{\mathrm{sf}} = \sigma_f^2 \mathbf{s}\mathbf{s}^H + \sigma_n^2 \mathbf{I}$.

III. Bound Expressions

Consider a data vector $\mathbf{y}$ and its likelihood function $f(\mathbf{y};\boldsymbol{\theta})$, which is dependent on a parameter vector $\boldsymbol{\theta}$. Under a set of regularity conditions, the CRLB for the mean square error of any unbiased estimator $\hat{\theta}_i(\mathbf{y})$ of the ith parameter θ_i is given by, e.g., [22]

$$E\left\{\left(\hat{\theta}_i(\mathbf{y}) - \theta_i\right)^2\right\} \geq \left[\mathbf{J}^{-1}(\boldsymbol{\theta})\right]_{ii} \quad (19)$$

where the matrix $\mathbf{J}(\boldsymbol{\theta})$ is known as the Fisher information matrix (FIM), which, for the current statistical model, is given by [22]

$$[\mathbf{J}(\boldsymbol{\theta})]_{ij} = \mathrm{tr}\left\{\mathbf{R}_{\mathbf{y}}^{-1}(\boldsymbol{\theta}) \frac{\partial \mathbf{R}_{\mathbf{y}}(\boldsymbol{\theta})}{\partial \theta_i} \mathbf{R}_{\mathbf{y}}^{-1}(\boldsymbol{\theta}) \frac{\partial \mathbf{R}_{\mathbf{y}}(\boldsymbol{\theta})}{\partial \theta_j}\right\} \quad (20)$$

[3]In addition to differences in the parameterization of $\mathbf{S}$, note that since, in [20], there is no temporal channel correlation, the Fisher information increases *proportionally* with time. However, for the temporal problem, this is not the case; the samples are statistically dependent. Thus, the covariance matrix dimension increases with the sample size, and the increase in the Fisher information now depends on "how fast" the channel correlation decreases, which motivates a specific analysis of the bound for the temporal case.

where $\mathrm{tr}\{\cdot\}$ denotes the trace of a matrix. The remainder of this section uses (20) and approximations thereof to obtain expressions for the CRLB for the time synchronization parameter in slow and fast fading channels.

A. Slow Fading

Recall that parameter vector for the slow fading case of (18) contains three elements: $\boldsymbol{\theta}^{\mathrm{sf}} = [\tau,\, \sigma_f^2,\, \sigma_n^2]^T$. It is not difficult to show that the constant modulus property of CPM signal yields a FIM of the form [23][4]

$$\mathbf{J}^{\mathrm{sf}} = \begin{bmatrix} J_{\tau\tau}^{\mathrm{sf}} & 0 & 0 \\ 0 & J_{\sigma_f^2\sigma_f^2}^{\mathrm{sf}} & J_{\sigma_f^2\sigma_n^2}^{\mathrm{sf}} \\ 0 & J_{\sigma_n^2\sigma_f^2}^{\mathrm{sf}} & J_{\sigma_n^2\sigma_n^2}^{\mathrm{sf}} \end{bmatrix} \quad (21)$$

which means that the error in the estimation of τ is *asymptotically uncorrelated* with the errors of the estimation of the nuisance parameters and that the bound on τ may be written as $\mathrm{CRLB}^{\mathrm{sf}}(\tau) = 1/J_{\tau\tau}^{\mathrm{sf}}$. Straightforward calculations indicate that $J_{\tau\tau}^{\mathrm{sf}}$ may be written in a form analogous to that for bearing estimation, e.g., [23]

$$J_{\tau\tau}^{\mathrm{sf}} = \frac{2N\rho^2}{1+N\rho} \mathbf{s}_\tau^H \mathbf{P}_{\mathbf{s}}^{\perp} \mathbf{s}_\tau, \quad \mathbf{P}_{\mathbf{s}}^{\perp} = \mathbf{I} - \frac{1}{N}\mathbf{s}\mathbf{s}^H \quad (22)$$

where $\mathbf{P}_{\mathbf{s}}^{\perp}$ is the projection matrix onto the subspace orthogonal to the signal subspace (spanned by $\mathbf{s}$), and $\mathbf{s}_\tau \equiv \partial\mathbf{s}/\partial\tau$. This implies that the bound is determined by the norm of the projection of $\mathbf{s}_\tau$ on the signal subspace's orthogonal complement and that for minimum error, the derivative of the signal vector $\mathbf{s}_\tau$ should be orthogonal to the signal vector itself. Note that for asymptotically high SNR, the bound tends to zero.

The bound can also be written in terms of the phase as

$$J_{\tau\tau}^{\mathrm{sf}} = \frac{2\rho^2}{1+N\rho} \left[N \sum_{i=0}^{N-1} \left(\frac{\partial}{\partial\tau}\varphi(iT_s - \tau, \boldsymbol{\eta})\right)^2 - \left(\sum_{i=0}^{N-1} \frac{\partial}{\partial\tau}\varphi(iT_s - \tau, \boldsymbol{\eta})\right)^2\right] \quad (23)$$

which, for MSK, yields, via (6)

$$J_{\tau\tau}^{\mathrm{sf}} = \frac{\rho^2}{1+N\rho}\frac{\pi^2}{2T_b^2} \times \left[N^2 - \left(\sum_{i=0}^{N-1} m_I(iT_s - \tau) m_Q(iT_s - \tau)\right)^2\right]. \quad (24)$$

[4]Note that calculation of the bound on τ (for either slow or fast fading) requires the elements of the (respective) data covariance to be differentiable with respect to τ. More specifically, the samples of the CPM signal should not occur at times where the complex envelope has no derivative. For MSK, for example, (6), this occurs every T_b. Therefore, in general, this analysis is valid for MSK, as long as the (unsynchronized) receiver does not sample exactly at the transition instances (which happens with probability zero). Moreover, many CPM formats have continuous derivatives with respect to the time [e.g., Gaussian MSK (GMSK)]; therefore, this question does not even arise.

B. Fast Fading

Bound expressions for the fast fading case are now presented. Begin by noting that application of the matrix inversion lemma to the data covariance $\mathbf{R_y}$ together with the constant modulus property of CPM (implying $\mathbf{S}^H\mathbf{S} = \mathbf{I}$) yields

$$\mathbf{R}_{\mathbf{y}}^{-1} = \frac{1}{\sigma_n^2}\left[\mathbf{I} - \frac{1}{\sigma_n^2}\,\mathbf{S}\left(\mathbf{R}_{\mathbf{f}}^{-1} + \frac{1}{\sigma_n^2}\,\mathbf{I}\right)^{-1}\mathbf{S}^H\right]. \tag{25}$$

Use of (25) in (20) followed by simple manipulations leads to the fact that, as in the slow fading case, the asymptotic error in the delay parameter is decoupled from those of the nuisance parameters (see Appendix B)

$$\mathbf{J} = \begin{bmatrix} J_{\tau\tau} & 0 & 0 & 0 \\ 0 & J_{\sigma_f^2\sigma_f^2} & J_{\sigma_f^2\sigma_n^2} & J_{\sigma_f^2\alpha} \\ 0 & J_{\sigma_n^2\sigma_f^2} & J_{\sigma_n^2\sigma_n^2} & J_{\sigma_n^2\alpha} \\ 0 & J_{\alpha\sigma_f^2} & J_{\alpha\sigma_n^2} & J_{\alpha\alpha} \end{bmatrix} \tag{26}$$

yielding $\mathrm{CRLB}(\tau) = J_{\tau\tau}^{-1}$. It is emphasized that this result is valid for any type of fading correlation (e.g., Jakes, AR) when the fading process is complex normal and of zero mean. In addition, note that this asymptotic decoupling both in the slow and fast fading scenarios implies that there is no inherent accuracy penalty due to the absence of *a priori* knowledge of the signal and noise power (as well as the channel correlation parameter for the fast fading case). To proceed, a variety of approximations are now considered.

1) Zero-Order High SNR Approximation: Begin by considering the "zero-order" high SNR approximation to the data covariance, which is similar to [20] and [24], by simply neglecting the noise term such that

$$\mathbf{R}_{\mathbf{y}}^{-1} \approx \mathbf{S}\mathbf{R}_{\mathbf{f}}^{-1}\mathbf{S}^H, \qquad \rho \gg 1. \tag{27}$$

Plugging (27) into (20) and using the fact that

$$\frac{\partial \mathbf{R}_{\mathbf{y}}(\boldsymbol{\theta})}{\partial\tau} = \frac{\partial}{\partial\tau}\left(\mathbf{S}\mathbf{R}_{\mathbf{f}}\mathbf{S}^H + \sigma_n^2\mathbf{I}\right) = \mathbf{S}_\tau\mathbf{R}_{\mathbf{f}}\mathbf{S}^H + \mathbf{S}\mathbf{R}_{\mathbf{f}}\mathbf{S}_\tau^H \tag{28}$$

yields the following expression for the FIM element for $J_{\tau\tau}$ at asymptotically high SNR:

$$J_{\tau\tau}^{\mathrm{High1}} = 2\cdot\mathrm{tr}\left\{\mathbf{S}\mathbf{R}_{\mathbf{f}}^{-1}\mathbf{S}^H\mathbf{S}_\tau\mathbf{R}_{\mathbf{f}}\mathbf{S}_\tau^H - \mathbf{S}_\tau\mathbf{S}_\tau^H\right\} \tag{29}$$

where $\mathbf{S}_\tau \equiv (\partial/\partial\tau)\,\mathbf{S}$. Remembering that $\mathbf{S}_{ii} = e^{j\varphi(iT_s-\tau,\boldsymbol{\eta})}$, the following diagonal matrix will be defined:

$$[\mathbf{A}]_{ii} \triangleq a_i = \left[\mathbf{S}\mathbf{S}_\tau^H\right]_{ii} = -j\,\frac{\partial}{\partial\tau}\,\varphi(iT_s-\tau,\boldsymbol{\eta}) \tag{30}$$

such that

$$\mathbf{S}_\tau\mathbf{S}_\tau^H = -\mathbf{A}^2, \quad [\mathbf{A}^2]_{ii} = -\left(\frac{\partial}{\partial\tau}\,\varphi(iT_s-\tau,\boldsymbol{\eta})\right)^2. \tag{31}$$

The second element in the trace in (29) yields

$$[2\mathbf{A}^2]_{ii} = -2\left[\mathbf{S}_\tau\mathbf{S}_\tau^H\right]_{ii} = -2\left(\frac{\partial}{\partial\tau}\,\varphi(iT_s-\tau,\boldsymbol{\eta})\right)^2 \tag{32}$$

and using $\mathrm{tr}\{\mathbf{XY}\} = \mathrm{tr}\{\mathbf{YX}\}$, we can write the first element of (29) as $\mathrm{tr}\{\mathbf{S}\mathbf{R}_{\mathbf{f}}^{-1}\mathbf{S}^H\mathbf{S}_\tau\mathbf{R}_{\mathbf{f}}\mathbf{S}_\tau^H\} = \mathrm{tr}\{\mathbf{A}\mathbf{R}_{\mathbf{f}}^{-1}\mathbf{A}^H\mathbf{R}_{\mathbf{f}}\}$. Tedious but straightforward calculations yield a final expression of the form (see Appendix C)

$$J_{\tau\tau}^{\mathrm{High1}} = \frac{2\alpha^2}{1-\alpha^2}\left[\sum_{i=1}^{N-2} a_i(2a_i^* - a_{i-1}^* - a_{i+1}^*) - a_0a_1^* - a_{N-1}a_{N-2}^* + a_0a_0^* + a_{N-1}a_{N-1}^*\right] \tag{33}$$

which can be seen to depend only on the transmitted sequence and the channel correlation parameter. Most importantly, in contrast to the slow fading case, it is evident from (33) that the bound on τ *does not* go to zero for asymptotically high SNR; there is an inherent asymptotic error generated due to the random fading channel process. It also appears that the bound is not valid when $\alpha = 1$ since $\mathbf{R_f}$ is a rank one matrix and is, therefore, noninvertible. If it is known *a priori* that $\alpha = 1$ (corresponding to *slow fading*), then the CRLB analysis is to be formulated accordingly as in Section III A.

For MSK, observe that

$$\left[\mathbf{S}_\tau^H\mathbf{S}\right]_{ii} \triangleq a_i = -j\,\frac{\pi}{2T_b}\,m_I(iT_s-\tau)m_Q(iT_s-\tau). \tag{34}$$

Plugging (34) into (29) yields

$$J_{\tau\tau}^{\mathrm{High1}}\cdot T_b^2 = \pi^2\,\frac{\alpha^2}{1-\alpha^2}\,[N-1-\gamma], \quad \gamma = \sum_{i=0}^{N-2} M[i]$$
$$M[i] = m_I(iT_s-\tau)m_I\left((i+1)T_s-\tau\right) \times m_Q(iT_s-\tau)m_Q\left((i+1)T_s-\tau\right) \tag{35}$$

where the placement of the T_b^2 factor on the right-hand side of (35) yields a bit period normalized version of the bound. It can be seen that $[N-1-\gamma]$ counts changes in the transmitted I and Q signal components. When there is a change in the bit values between consecutive samples in either the I or Q components, the associated $M[i]$ equals -1; otherwise, $M[i]$ equals 1 . Depending on the transmitted bit sequence, the value of γ can range between $N-1$ for the worst-case sequence and $-(N-1)$ for the best-case sequence (see Section VI).

2) First-Order High SNR Approximation: A "first-order" high SNR approximation to the inverse of the data covariance can be obtained by writing the first-order Taylor expansion for $(\mathbf{I}+\sigma_n^2\mathbf{R}_{\mathbf{f}}^{-1})^{-1}$ around $\tilde{\rho} = 1/\rho = 0$ (similarly to [15] and [20])[5]

[5]Actually, $\sigma_n^2\mathbf{R}_{\mathbf{f}}^{-1} = (1/\rho(1-\alpha^2))\,\overline{\mathbf{R}_{\mathbf{f}}^{-1}}$, $\overline{\mathbf{R}_{\mathbf{f}}^{-1}} = \sigma_f^2(1-\alpha^2)\mathbf{R}_{\mathbf{f}}^{-1}$ [see (16)], and therefore, the first-order high SNR approximation requires that $\rho(1-\alpha^2)\to\infty$.

$$(\mathbf{I}+\sigma_n^2\mathbf{R}_\mathbf{f}^{-1})^{-1}\approx\mathbf{I}-\sigma_n^2\mathbf{R}_\mathbf{f}^{-1}. \tag{36}$$

Now, $\mathbf{R}_\mathbf{y}^{-1}$ can be approximated as

$$\mathbf{R}_\mathbf{y}^{-1}\approx\mathbf{S}\mathbf{R}_\mathbf{f}^{-1}\mathbf{S}^H-\sigma_n^2\mathbf{S}\mathbf{R}_\mathbf{f}^{-2}\mathbf{S}^H. \tag{37}$$

Inserting (37) and (28) in (20) and using the fact that $\mathbf{S}\mathbf{S}_\tau^H\mathbf{S}\mathbf{S}_\tau^H=-\mathbf{S}_\tau^H\mathbf{S}_\tau$ yields, after simple manipulations

$$J_{\tau\tau}^{\text{High2}}=J_{\tau\tau}^{\text{High1}}-\frac{2\sigma_f^2}{\rho}\,\text{tr}\left\{\mathbf{S}\mathbf{R}_\mathbf{f}^{-2}\mathbf{S}^H\mathbf{S}_\tau\mathbf{R}_\mathbf{f}\mathbf{S}_\tau^H-\mathbf{S}_\tau\mathbf{S}_\tau^H\mathbf{R}_\mathbf{f}^{-1}\right\}. \tag{38}$$

The first-order high SNR expression is seen to be the zero-order high SNR expression minus an SNR dependent term.

3) Low SNR Approximation: First, note that the constant modulus property enables expression of the inverse of the data covariance as

$$\mathbf{R}_\mathbf{y}^{-1}=\left[\mathbf{S}(\mathbf{R}_\mathbf{f}+\sigma_n^2\mathbf{I})\mathbf{S}^H\right]^{-1}=\frac{1}{\sigma_n^2}\,\mathbf{S}\left(\mathbf{I}+\frac{1}{\sigma_n^2}\mathbf{R}_\mathbf{f}\right)^{-1}\mathbf{S}^H.$$

A low SNR approximation can be obtained by performing a first-order Taylor series expansion of $(\mathbf{I}+(1/\sigma_n^2)\mathbf{R}_\mathbf{f})^{-1}$ about $\rho=0$, yielding

$$\mathbf{R}_\mathbf{y}^{-1}\approx\frac{1}{\sigma_n^2}\left[\mathbf{I}-\frac{1}{\sigma_n^2}\,\mathbf{S}\mathbf{R}_\mathbf{f}\mathbf{S}^H\right]\qquad\rho\ll 1. \tag{39}$$

Plugging (39) and (28) into (20) yields the following low SNR approximation for the Fisher information:

$$J_{\tau\tau}^{\text{Low}}=2\left(\frac{1}{\sigma_n^2}\right)^2\text{tr}\left\{\mathbf{R}_\mathbf{f}\left(\mathbf{R}_\mathbf{f}\mathbf{S}_\tau^H\mathbf{S}_\tau-\mathbf{S}^H\mathbf{S}_\tau\mathbf{R}_\mathbf{f}\mathbf{S}_\tau^H\mathbf{S}\right)\right\}. \tag{40}$$

Using (30) and (31) gives

$$J_{\tau\tau}^{\text{Low}}=2\rho^2\left[\sum_{i=0}^{N-1}\sum_{j=0}^{N-1}(a_ia_j-a_i^2)\alpha^{2|i-j|}\right]. \tag{41}$$

Unlike the zero-order high SNR case, $J_{\tau\tau}^{\text{Low}}$ depends on SNR and the transmitted sequence.

IV. Bound Properties

This section uses the results of the previous section to obtain a series of bound properties for the slow and fast fading channels.

A. Slow Fading

Property 1: For sufficiently high SNR, the bound on delay estimation for slow fading is approximately inversely proportional to SNR.

Proof: Follows from direct inspection of (22).

Property 2: The bound on delay estimation for slow fading is monotonically nonincreasing function of the sample size N.

Proof: See Appendix D.

B. Fast Fading

Property 1: In contrast to the slow fading case, for low SNR, the fast fading bound is proportional to $(1/\rho^2)$ (decreasing rapidly with SNR), whereas for high SNR, the fast fading bound is proportional to $\rho/(\rho-\kappa)$ for some constant κ (decreasing much more slowly with SNR).

Proof: The low and high SNR parts of the property follow immediately from (40) and (38), respectively.

Property 2: At high SNR, the bound on delay estimation for fast fading is monotonically nonincreasing function of the sample size N.

Proof: Examining (33), it is seen that N appears only in the signal-dependent factor. Define

$$Z_N'\triangleq\sum_{i=1}^{N-2}a_i(2a_i^*-a_{i-1}^*-a_{i+1}^*)-a_0a_1^*-a_{N-1}a_{N-2}^*+a_0a_0^*+a_{N-1}a_{N-1}^*. \tag{42}$$

To show that $Z_N'-Z_{N-1}'\geq 0$, write

$$\begin{aligned}Z_N'-Z_{N-1}'&=a_{N-2}a_{N-2}^*-a_{N-2}a_{N-1}^*\\&\quad+a_{N-1}a_{N-1}^*-a_{N-1}a_{N-2}^*\\&=(a_{N-2}-a_{N-1})(a_{N-2}^*-a_{N-1}^*)\\&=|a_{N-2}-a_{N-1}|^2\geq 0\end{aligned}$$

which completes the proof.

Property 3: For sufficiently low and sufficiently high SNR, the bound on delay estimation is a monotonically decreasing function of the channel correlation parameter (α) which varies from infinity (at $\alpha=0$) to the slow fading bound (at $\alpha=1$).

Proof: Monotonicity can be proven directly from (33), which (at least for high SNR) indicates that the bound's dependence on the channel correlation parameter is contained in the term $2\alpha^2/(1-\alpha^2)$, which, for $\alpha\in[0,1)$, is a monotonically increasing function of α.

The fact that the bound tends to infinity at $\alpha=0$ is also seen from the above channel-dependent term or, more generally, by the fact that as $\alpha\to 0$, $\mathbf{R}_\mathbf{f}$ can be approximated as $\mathbf{R}_\mathbf{f}\approx\sigma_f^2\mathbf{I}$ such that

$$\begin{aligned}\frac{\partial\mathbf{R}_\mathbf{y}(\boldsymbol{\theta})}{\partial\tau}&=\frac{\partial}{\partial\tau}\left(\mathbf{S}\mathbf{R}_\mathbf{f}\mathbf{S}^H+\sigma_n^2\mathbf{I}\right)\\&=\mathbf{S}_\tau\mathbf{R}_\mathbf{f}\mathbf{S}^H+\mathbf{S}\mathbf{R}_\mathbf{f}\mathbf{S}_\tau^H\\&\approx\sigma_f^2\left(\mathbf{S}_\tau\mathbf{S}^H+\mathbf{S}\mathbf{S}_\tau^H\right)\equiv\mathbf{0}\end{aligned} \tag{43}$$

where the last equality follows from the constant modulus property of CPM. This means that as $\alpha\to 0$, $J_{\tau\tau}\to 0$ or, equivalently, that the bound is infinite. This property is very intuitive since, as α goes to zero, the channel becomes increasingly more white—decorrelating the signal samples to the point where there is no structure on which an estimator can synchronize.

In the case of asymptotically high SNR, convergence of the fast fading bound to the slow fading bound as α tends to one again follows from the bound term $2\alpha^2/(1-\alpha^2)$ of (33), which approaches infinity. This implies that the CRLB tends to zero, as does the slow fading bound for asymptotically increasing SNR.

For low SNR, monotonicity can be proven directly from the fast-fading FIM element for τ, $J_{\tau\tau}^{\mathrm{Low}}(\boldsymbol{\eta})$, which is given by (41). Next, to prove convergence to the slow fading bound, examine again (41). When α approaches 1, (41) becomes

$$\lim_{\alpha\to 1} J_{\tau\tau}^{\mathrm{Low}} = 2\rho^2 \left[\sum_{i=0}^{N-1}\sum_{j=0}^{N-1}(a_i a_j - a_i^2)\right]. \tag{44}$$

Inserting a_i as defined in (30), we can write

$$\lim_{\alpha\to 1} J_{\tau\tau}^{\mathrm{Low}} = 2\rho^2 \left[N\sum_{i=0}^{N-1}\left(\frac{\partial}{\partial\tau}\varphi(iT_s-\tau,\boldsymbol{\eta})\right)^2 - \left(\sum_{i=0}^{N-1}\frac{\partial}{\partial\tau}\varphi(iT_s-\tau,\boldsymbol{\eta})\right)^2\right]. \tag{45}$$

Examining $J_{\tau\tau}^{\mathrm{sf}}$ expressed in terms of the phase (23)

$$\lim_{\alpha\to 1} J_{\tau\tau}^{\mathrm{sf}} = \frac{2\rho^2}{1+N\rho}\left[N\sum_{i=0}^{N-1}\left(\frac{\partial}{\partial\tau}\varphi(iT_s-\tau,\boldsymbol{\eta})\right)^2 - \left(\sum_{i=0}^{N-1}\frac{\partial}{\partial\tau}\varphi(iT_s-\tau,\boldsymbol{\eta})\right)^2\right] \tag{46}$$

we see that as $\rho \to 0$, $J_{\tau\tau}^{\mathrm{Low}^{-1}} \to J_{\tau\tau}^{\mathrm{sf}^{-1}}$ (since $\lim_{\rho\to 0} 1+N\rho = 1$), and the resulting expression is identical to (45), thus completing proof of the property.

Property 4 (for MSK Only): For asymptotically high SNR, the bound on delay estimation for MSK over a fast-fading channel decreases as the sampling rate increases.

Proof: See Appendix A

V. Numerical Example

This section presents numerical examples that illustrate the behavior of the CRLB on τ as a function of SNR, time-doppler product, sampling rate, and sample size. A nominal MSK modulation scenario is considered with a bit rate of $R_b = 1/T_b = 100$ KBPS, a sampling rate of $T_s = T_b/2$, an AR1 fading channel model with $\alpha = 0.73$ (corresponding to $B_dT_b = 0.1$), an SNR of $\rho = 15$ dB, and an alternating bit sequence of length $K = 31$ bits. Graphs of the exact and approximate forms of the square root of the CRLB are plotted as one of the above listed parameters is varied from its nominal value.

Begin with Fig. 2, which presents a comparison of the bound on delay estimation calculated with the Jakes and the AR1 correlation model. Examining the figure, it can be seen that while the Jakes bound is lower than the AR1 bound, both exhibit the same *type* of behavior versus SNR. This was also found to be the case for a wide variety of scenarios (not shown).

Next, Fig. 3 presents the bound on delay estimation versus SNR. Fig. 3(a) plots the bound for SNRs ranging from -15 to 30 dB, whereas Fig. 3(b) zooms in on the high SNRs. Examining the figure, we observe a slow and fast fading CRLB dependence on SNR as predicted by Property 1 in Sections IV-A and B, respectively. In particular, note how the

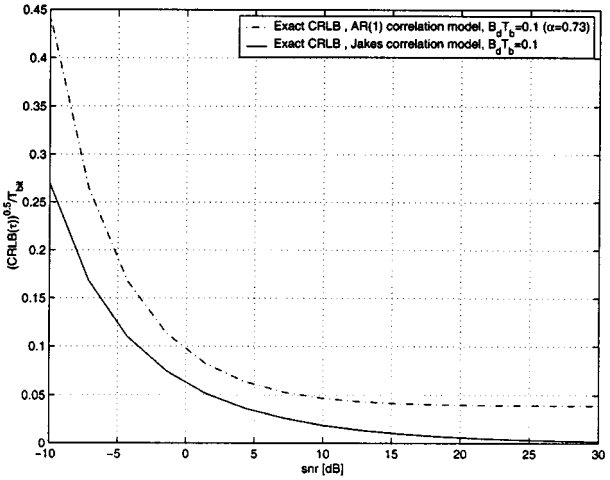

Fig. 2. Exact bounds on delay estimation for DA time synchronization with a fast fading channel versus SNR size for the Jakes and AR1 correlation model $R_b = 100$ KBPS, SNR $= 15$ dB, $T_s = (T_b/2)$, $B_dT_b = 0.1$.

fast-fading bound decreases more rapidly for low SNR than the slow-fading bound. At higher SNR, however, the fast-fading bound decreases more slowly than the slow-fading bound. We can also see [Fig. 3(b)] that the fast-fading bound arrives at some nonzero asymptotic value (see Property 1, Section IV-B) for asymptotically increasing SNR, whereas the slow-fading bound drops to zero as SNR increases. Additionally, we observe that the first-order high SNR approximation is better than the zero-order high SNR approximation for SNRs that are higher than $\sim$14 dB. However, for lower SNRs, the first-order approximation yields performance that is far inferior to that of the zero-order approximation. To understand why, recall that the zero-order high SNR approximation for the inverse of the correlation matrix is $\mathbf{R}_{\mathbf{y}}^{-1} \approx \mathbf{S}\mathbf{R}_{\mathbf{f}}^{-\mathbf{1}}\mathbf{S}^H$. This formula is meaningful at all SNRs, which implies that the approximate bound will deteriorate gradually as the SNR decreases. The first-order high SNR approximation for the inverse of the correlation matrix is $\mathbf{R}_{\mathbf{y}}^{-1} \approx \mathbf{S}\mathbf{R}_{\mathbf{f}}^{-\mathbf{1}}\mathbf{S}^H - \sigma_n^2\mathbf{S}\mathbf{R}_{\mathbf{f}}^{-\mathbf{2}}\mathbf{S}^H$. This approximation is better than the zero-order approximation at moderate to high SNR; however, at some point when the SNR decreases, the second term becomes dominant, making $\mathbf{R}_{\mathbf{y}}^{-1}$ negative definite, which means that the approximation collapses. The SNR at which the approximation collapses is also determined by the correlation parameter α [we require that $\rho(1-\alpha^2)$ will be large enough]. At SNRs near the collapse of the approximation, the first-order approximation will deteriorate faster than the zero-order high SNR approximation. Finally, we note that for sufficiently high SNR, the SNR does not have a significant effect on the fast-fading bound on delay estimation, and the zero-order high SNR approximation gives quite good results, even for SNRs as low as 10 dB.

Fig. 4 presents the behavior of the CRLB versus the sample size N. It is seen that as N increases, the bound decreases for both slow-fading and fast-fading channels, as predicted by Property 2 in Sections IV-A and B for slow fading and fast fading, respectively. Note that the bound is not necessarily a monotonically decreasing function as in Fig. 4 and that there are sequences for which the inclusion of additional symbols

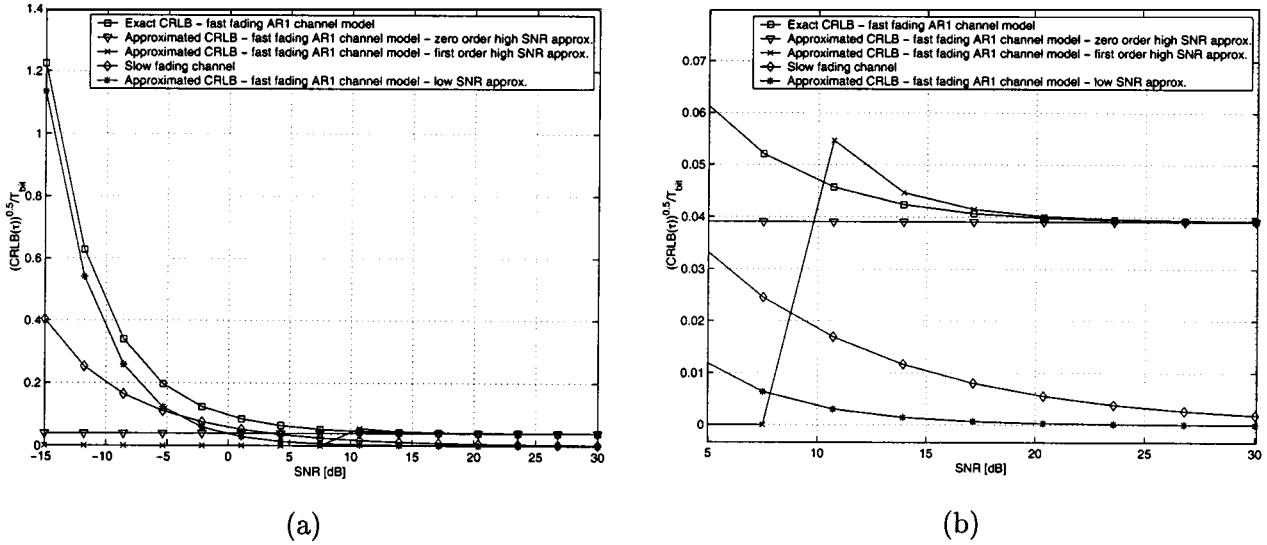

Fig. 3. Bounds on delay estimation for DA time synchronization with a fast-fading channel versus SNR, $R_b = 100$ KBPS, $K = 31$ bits, $T_s = (T_b/2)$, $B_dT_b = 0.1$.

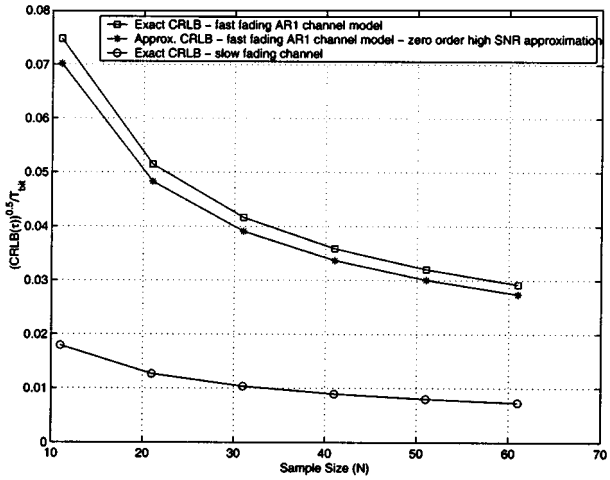

Fig. 4. Bounds on delay estimation for DA time synchronization with a fast-fading channel versus sample size, $R_b = 100$ KBPS, SNR$= 15$ dB, $T_s = (T_b/2)$, $B_dT_b = 0.1$.

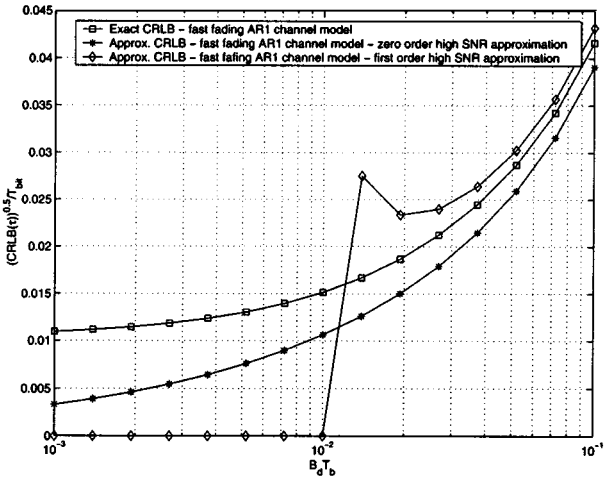

Fig. 5. Bounds on delay estimation for DA time synchronization with a fast-fading channel versus time-Doppler product, $R_b = 100$ KBPS, $K = 31$ bits, $T_s = (T_b/2)$, SNR $= 15$ dB.

will not decrease the bound. We give an example of such a "bad" sequence in Section VI.

Next, Fig. 5 presents the dependence of the bound on the time-Doppler product. The figure indicates that the bound increases as the time-Doppler product increases. This is consistent with Property 3 of Section IV-B, which predicts that as α increases toward unity (i.e., the time-Doppler product approaches zero for fixed bit rate), the bound decreases, whereas as α decreases toward zero (i.e., the time-Doppler product increases to infinity), the bound increases to infinity. The time-Doppler product has a significant effect on the bound. This is because the fading becomes more uncorrelated as B_dT_b increases, such that the received signal phase becomes increasingly more white, making it difficult to extract timing information. We also see from Fig. 5 that the first-order high SNR approximation breaks down, even though only α is varied, whereas the SNR remains constant. The reason is that the first-order high SNR approximation actually requires that $\rho(1-\alpha^2)$ will be large enough for the approximation to be valid. As B_dT_b decreases, α increases toward unity, and the first-order high SNR assumption is violated. Finally, consider the bound on delay estimation as a function of the sampling rate. Fig. 6 shows that as the sampling rate increases, the bound on delay estimation decreases, as indicated by Property 4 of Section IV-B.

VI. Synchronization Sequence Design

It is clear from the preceding sections that the bounds on the time delay parameter depend, in general, on the transmitted bit sequence. An interesting question that arises is how the choice of transmitted bit sequence can help improve synchronization performance. Begin by reconsidering the asymptotic high SNR bound expression (35) when $T_s = T_b$ (implying $N = K - 1$). To minimize the bound, γ is to be as negative as possible. For $T_s = T_b$, $M[i]$ consists of two samples of the same bit that multiply to one and two samples from two consecutive bits (see Fig. 7). If γ is to be as negative as possible, the elements from

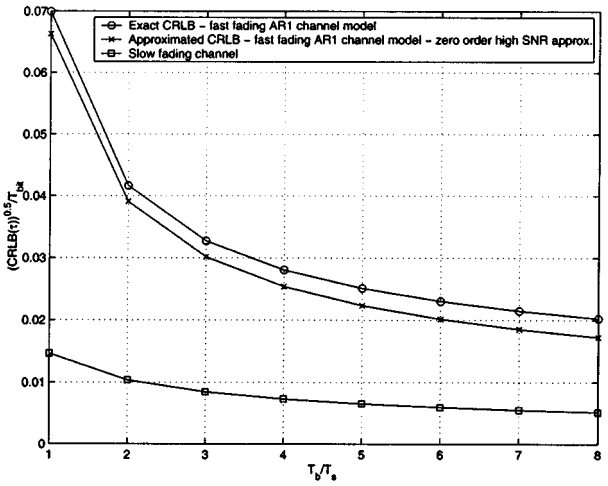

Fig. 6. Bounds on delay estimation for DA time synchronization with a fast-fading channel versus sampling rate, $R_b = 100$ KBPS, $K = 31$ bits, $T_s = (T_b/2)$, SNR = 15 dB.

consecutive bits should have different signs. This means that both the I and the Q branches should have alternating bits

$$bits\{m_I\} = -1,\ 1,\ -1,\ 1,\ -1,\ 1,\ \ldots$$
$$bits\{m_Q\} = -1,\ 1,\ -1,\ 1,\ -1,\ 1,\ \ldots \tag{47}$$

such that the transmitted synchronization bits are

$$\mathbf{u}_{best} = [-1,\ -1,\ 1,\ 1,\ -1,\ -1,\ 1,\ 1,\ -1,\ -1,\ \ldots]^T. \tag{48}$$

In this case, (35) yields

$$\mathrm{CRLB}(\tau|\mathbf{u}_{best}) = \left[J_{\tau\tau}^{\mathrm{High1}}(\mathbf{u}_{best})\right]^{-1} = \frac{1}{2(N-1)}\,\frac{T_b^2}{\pi^2}\,\frac{1-\alpha^2}{\alpha^2}. \tag{49}$$

The physical meaning of the choice (48) is that the transmitted MSK signal consists of frequencies that alternate between F_H and F_L every T_b seconds (which is the fastest switching this modulation allows). Obviously, fast switching between two frequencies is the best time synchronization signal that can be generated by MSK modulation.

Now, let us look for the worst-case signal on which to synchronize. For this signal, we want γ to be positive and large such that the Fisher information is minimized. Following the same reasoning, it is clear that an obvious choice would be that of choosing all the I bits to be the same and all the Q bits to be the same. As an example, we can choose

$$bits\{m_I\} = -1,\ -1,\ -1,\ -1,\ -1,\ -1,\ \ldots$$
$$bits\{m_Q\} = 1,\ 1,\ 1,\ 1,\ 1,\ 1,\ \ldots \tag{50}$$

such that

$$\mathbf{u}_{worst} = [-1,\ 1,\ -1,\ 1,\ -1,\ 1,\ -1,\ 1,\ -1,\ 1,\ \ldots]^T. \tag{51}$$

This corresponds to transmission of only a sinusoid of frequency F_L, which, in the absence of *a priori* knowledge of the channel phase, makes time synchronization impossible. Here, $\gamma = N - 1$, and the bound for this case is infinite.

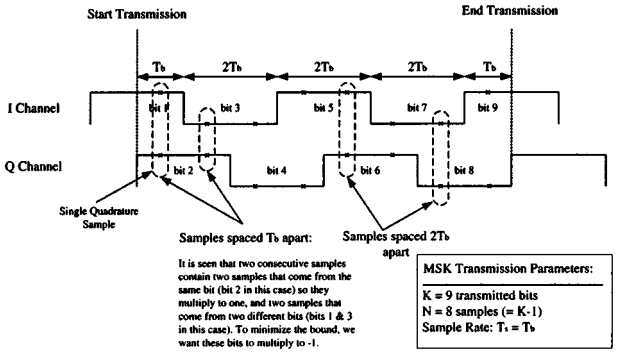

Fig. 7. I and Q channel for best MSK sequence sampled at $T_s = T_b$. $K = 9$, $N = 8$.

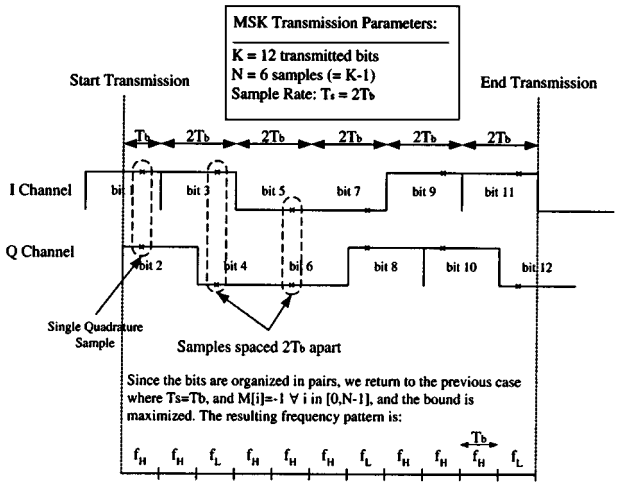

Fig. 8. I and Q channel for best MSK sequence sampled at $T_s = 2T_b$. $K = 12$, $N = 6$.

It is important to note that the best and worst sequences are not "universal" but depend on the sampling rate. For example, if we sample the best sequence derived for $T_s = T_b$ with $T_s = 2T_b$, each of the four factors of $M[i]$ comes from different bits (see Fig. 7). Since the sequence on each branch is alternating, the total multiplications yield $+1$ for all $M[i]$s resulting in an infinite bound. The best case is when the alterations take place in pairs. Such a signal is given in Fig. 8. The physical meaning of such a choice is that at every sample, we get a different frequency and not necessarily at every T_b interval. The transmitted bits will now be

$$bits\{m_I\} = 1,\ 1,\ -1,\ -1,\ 1,\ 1,\ \ldots$$
$$bits\{m_Q\} = 1,\ -1,\ -1,\ 1,\ 1,\ -1,\ \ldots$$

such that

$$\mathbf{u}_{best} = [1,\ 1,\ 1,\ -1,\ -1,\ -1,\ -1,\ 1,\ 1,\ 1,\ 1,\ -1\cdots]^T.$$

As a final note, since the sequence design procedure based on the bound is derived under the AR1 channel correlation model, we present in Fig. 9 a comparison of the bound values for all 11 bits sequences derived for the Jakes and AR1 correlation models (the other scenario parameters are the same as in the nominal scenario of Section V). Although there is a clear absolute difference in the two bounds, it is found that the ordering of bound magnitude versus sequence index is identical for the two models, implying that the results derived under the AR1 model also apply to the Jakes correlation model. Finally,

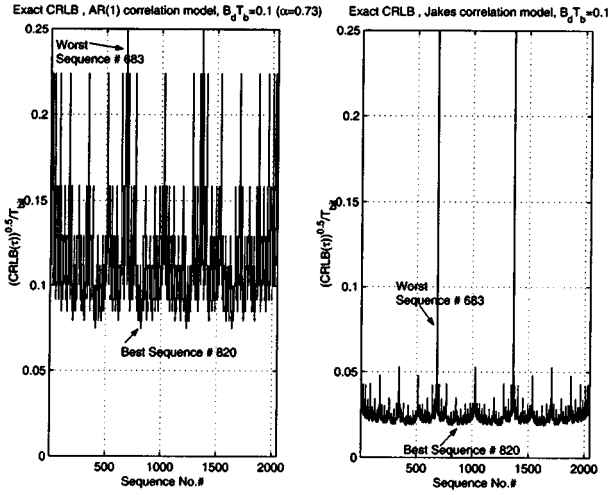

Fig. 9. Comparison for CRLB evaluated for all 11 bit MSK sequences. $T_s = (T_b/2)$, $B_dT_b = 0.1$, SNR = 15 dB, $\alpha = 0.73$, $K = 11$ bits, $R_b = 100$ KBPS.

note the importance of good sequence design; in addition to the four worst sequences with infinite bound, the other sequences possess bound values that are considerably above the minimal bound. Thus, care should be exercised in choosing the synchronization sequence.

VII. Conclusions

This paper has investigated the inherent limitations involved with DA time synchronization of CPM signals over time-selective fading channels. Exact and more intuitive approximate forms of the CRLB were presented for both CPM in general and MSK in particular. A number of properties that highlight how the bound depends on key parameters such as SNR, sampling rate, and time-Doppler product were derived. The results were compared with the corresponding slow fading bound, and a number of important differences were found. Analytical results were illustrated via several numerical examples. Finally, an application of the bound was presented for optimum synchronization sequence design. Current work focuses on the design and analysis of procedures for synchronization of CPM signals in time-selective channels.

Appendix A
Proof of Property 4

As seen from (35), the FIM element consists of a channel-dependent factor and a signal-dependent factor. Increasing the sampling rate from, say, the minimum rate for data detection of $T_s^{-1} = (2T_b)^{-1}$, up to $T_s^{-1} = T_b^{-1}$, increases (or at least does not decrease) the signal dependent factor $[N - 1 - \gamma]$ in (35) (which, as is shown in Section VI, for the appropriate sequence can decrease the overall bound). To understand why, observe that there are, in general, three basic combinations of I and Q bits, which are depicted in Fig. 10. All other combinations can be derived by multiplying the I and/or Q channels by -1. Such multiplication, however, will not change the evaluation of $M[i]$ [see (35)]. We will now examine what happens to $N - 1 - \gamma$ for each of these basic combinations when the sampling rate is increased from $T_s^{-1} = (2T_b)^{-1}$ up to $T_s^{-1} = T_b^{-1}$ with the aid of Fig. 10.

For the combination (a), we have $M[i] = -1$ for $T_s = 2T_b$. For $T_s = T_b$, we have an additional sample with $M[i] = 1$ (the first two bits) so that $N - 1 - \gamma$ is decreased by one because of the new $M[i]$ but is also increased by one due to the addition of a new sample; thus, in total, increasing the sampling rate did not change $N - 1 - \gamma$.

For the combination (b), since each branch has identical bits, it is obvious that the $M[i]$ is always one, and increasing the sampling rate will not change the total of $N - 1 - \gamma$.

Finally, for combination (c), we have $M[i] = 1$ for $T_s = 2T_b$. For $T_s = T_b$, we have $M[i] = -1$, and thus, $N - 1 - \gamma$ was increased by 2 due to the increase in sampling rate. In conclusion, we see that $N - 1 - \gamma$ may only increase when the sampling rate in increased.

Increasing the sampling rate from $T_s^{-1} = (2T_b)^{-1}$ up to $T_s^{-1} = T_b^{-1}$ also increases α (i.e., higher channel sample correlation), which, in turn, decreases the overall bound. Increasing the sampling rate above $T_s^{-1} = T_b^{-1}$ will not further increase $[N - 1 - \gamma]$. To understand why, note that the bound on time synchronization is related to changes in the transmitted signal through the $M[i]$s. Now, observe that $T_s^{-1} = T_b^{-1}$ is the lowest sampling rate for which all the changes in the signals are accounted for by the $M[i]$s [see (35) and Fig. 11]. Therefore, at $T_s^{-1} = T_b^{-1}$, we have all existing transition instances included in γ. Increasing the sampling rate above $T_s^{-1} = T_b^{-1}$ will not reveal new transitions. We will have additional samples, but since all the transitions are already accounted for, these samples appear in the middle of the bit intervals; they do not reveal new transitions. Therefore, for these new samples, $M[i] = 1$, and γ is increased by one for each of these new samples. However, $N - 1$ is also increased by one for each of these new samples; therefore, the two additions nullify each other, thus, not improving synchronization. However, α does continue to increase as the sampling rate increases. This means that no additional information can be extracted from the signal for these high sampling rates, and the improvement in the bound for these rates is only because we can better evaluate the effect of the channel on the signal.

Appendix B
Derivation of the Cross-Covariance Elements of $\mathbf{J} - J_{\tau\sigma_n^2}$, $J_{\tau\sigma_f^2}$ and $J_{\tau\alpha}$ for Fast Fading Case

1. Calculation of $J_{\alpha\tau}$:

Recall that

$$J_{\alpha\tau} = \mathrm{tr}\left\{\mathbf{R}_\mathbf{y}^{-1}\frac{\partial \mathbf{R}_\mathbf{y}}{\partial \alpha}\mathbf{R}_\mathbf{y}^{-1}\frac{\partial \mathbf{R}_\mathbf{y}}{\partial \tau}\right\}.$$

Using (14) and (25) and denoting $\mathbf{R}_\mathbf{y}^{(\alpha)} \triangleq \partial \mathbf{R}_\mathbf{y}/\partial\alpha$, $\mathbf{S}_\tau \triangleq \partial \mathbf{S}/\partial\tau$, we have

$$J_{\alpha\tau} = \mathrm{tr}\left\{\frac{1}{\sigma_n^2}\left[\mathbf{I} - \frac{1}{\sigma_n^2}\mathbf{S}\left(\mathbf{R}_\mathbf{f}^{-1} + \frac{1}{\sigma_n^2}\mathbf{I}\right)^{-1}\mathbf{S}^H\right]\mathbf{R}_\mathbf{y}^{(\alpha)} \times \frac{1}{\sigma_n^2}\left[\mathbf{I} - \frac{1}{\sigma_n^2}\mathbf{S}\left(\mathbf{R}_\mathbf{f}^{-1} + \frac{1}{\sigma_n^2}\mathbf{I}\right)^{-1}\mathbf{S}^H\right] \times \left(\mathbf{S}_\tau\mathbf{R}_\mathbf{f}\mathbf{S}^H + \mathbf{S}\mathbf{R}_\mathbf{f}\mathbf{S}_\tau^H\right)\right\}.$$

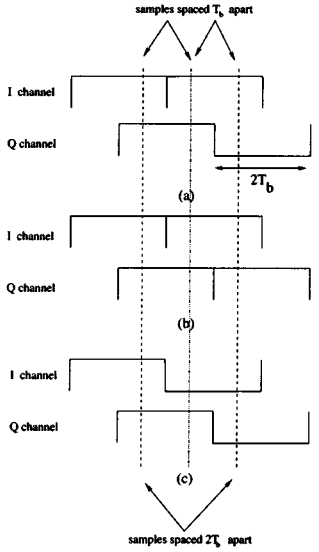

Fig. 10. Basic combinations of the I and Q bits for MSK transmission.

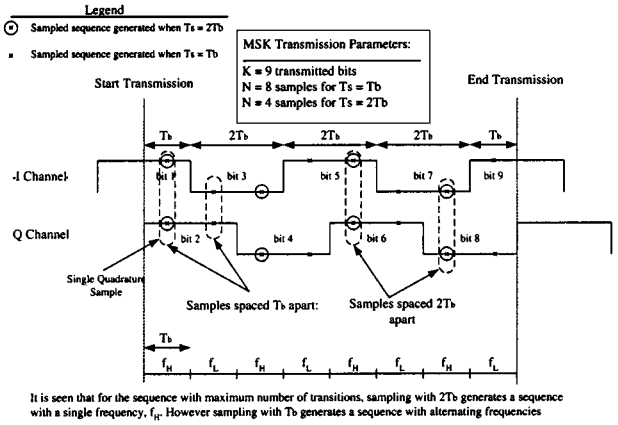

Fig. 11. I and Q channels for (best) MSK sequence for both $T_s = T_b$ and $T_s = 2T_b$. $K = 9$.

Defining $\mathbf{Z} = (\mathbf{R}_\mathbf{f}^{-1} + (1/\sigma_n^2)\,\mathbf{I})^{-1}$ and $\partial\mathbf{R}_\mathbf{f}/\partial\alpha \triangleq \mathbf{R}_\mathbf{f}^{(\alpha)}$, we have $\mathbf{R}_\mathbf{y}^{(\alpha)} = \mathbf{S}\mathbf{R}_\mathbf{f}^{(\alpha)}\mathbf{S}^H$. Recalling that $\mathbf{S}\mathbf{S}^H = \mathbf{I}$ and properties of the trace operation, we can expand $J_{\alpha\tau}$ as

$$J_{\alpha\tau} = \left(\frac{1}{\sigma_n^2}\right)^2 \mathrm{tr}\left\{\left[\mathbf{R}_\mathbf{f}^{(\alpha)}\mathbf{S}^H\mathbf{S}_\tau\mathbf{R}_\mathbf{f} + \mathbf{R}_\mathbf{f}^{(\alpha)}\mathbf{R}_\mathbf{f}\mathbf{S}_\tau{}^H\mathbf{S}\right]\right.$$
$$- \frac{1}{\sigma_n^2}\left[\mathbf{Z}\mathbf{R}_\mathbf{f}^{(\alpha)}\mathbf{S}^H\mathbf{S}_\tau\mathbf{R}_\mathbf{f} + \mathbf{Z}\mathbf{R}_\mathbf{f}^{(\alpha)}\mathbf{R}_\mathbf{f}\mathbf{S}_\tau{}^H\mathbf{S}\right]$$
$$- \frac{1}{\sigma_n^2}\left[\mathbf{R}_\mathbf{f}^{(\alpha)}\mathbf{Z}\mathbf{S}^H\mathbf{S}_\tau\mathbf{R}_\mathbf{f} + \mathbf{R}_\mathbf{f}^{(\alpha)}\mathbf{Z}\mathbf{R}_\mathbf{f}\mathbf{S}_\tau{}^H\mathbf{S}\right]$$
$$\left. + \left(\frac{1}{\sigma_n^2}\right)^2 \mathbf{Z}\mathbf{R}_\mathbf{f}^{(\alpha)}\mathbf{Z}\left[\mathbf{S}^H\mathbf{S}_\tau\mathbf{R}_\mathbf{f} + \mathbf{R}_\mathbf{f}\mathbf{S}_\tau{}^H\mathbf{S}\right]\right\}.$$

Now, if $\mathbf{D}$ is a diagonal matrix and $\mathbf{A}$ and $\mathbf{B}$ are symmetric matrices, then

$$\mathrm{tr}\{\mathbf{ABD}\} = \mathrm{tr}\{\mathbf{BAD}\} \tag{B.1}$$

so that $J_{\alpha\tau}$ can also be written as

$$J_{\alpha\tau} = \mathrm{tr}\left\{\left[\mathbf{R}_\mathbf{f}^{(\alpha)} - \frac{1}{\sigma_n^2}\mathbf{Z}\mathbf{R}_\mathbf{f}^{(\alpha)} - \frac{1}{\sigma_n^2}\mathbf{R}_\mathbf{f}^{(\alpha)}\mathbf{Z}\right.\right.$$
$$\left.\left. \times \left(\frac{1}{\sigma_n^2}\right)^2 \mathbf{Z}\mathbf{R}_\mathbf{f}^{(\alpha)}\mathbf{Z}\right] \times \left[\mathbf{S}^H\mathbf{S}_\tau + \mathbf{S}_\tau^H\mathbf{S}\right]\mathbf{R}_\mathbf{f}\right\}\left(\frac{1}{\sigma_n^2}\right)^2.$$

Next, examine $\mathbf{S}^H\mathbf{S}_\tau + \mathbf{S}_\tau^H\mathbf{S}$. Since $\mathbf{S}$ is a diagonal matrix, so are $\mathbf{S}^H\mathbf{S}_\tau$ and $\mathbf{S}_\tau^H\mathbf{S}$. The ith diagonal element of $\mathbf{S}^H\mathbf{S}_\tau$, for example, is

$$[\mathbf{S}^H\mathbf{S}_\tau]_{ii} = e^{-j\varphi(iT_s-\tau,\boldsymbol{\eta})}\frac{\partial}{\partial\tau}e^{j\varphi(iT_s-\tau,\boldsymbol{\eta})}$$
$$= j\frac{\partial}{\partial\tau}\varphi(iT_s-\tau,\boldsymbol{\eta}).$$

However, the ith diagonal element of $\mathbf{S}_\tau^H\mathbf{S}$ is given by

$$\left[\mathbf{S}_\tau^H\mathbf{S}\right]_{ii} = \left(\frac{\partial}{\partial\tau}e^{-j\varphi(iT_s-\tau,\boldsymbol{\eta})}\right)e^{j\varphi(iT_s-\tau,\boldsymbol{\eta})}$$
$$= -j\frac{\partial}{\partial\tau}\varphi(iT_s-\tau,\boldsymbol{\eta}) = -\left[\mathbf{S}^H\mathbf{S}_\tau\right]_{ii}.$$

Therefore

$$\mathbf{S}^H\mathbf{S}_\tau + \mathbf{S}_\tau^H\mathbf{S} \equiv \mathbf{0} \tag{B.2}$$

driving the entire expression for $J_{\alpha\tau}$ to zero.

The calculation of $J_{\tau\sigma_f^2}$ and $J_{\tau\sigma_n^2}$ follows along the same lines as the calculation of $J_{\alpha\tau}$.

Appendix C
Calculation of $J_{\tau\tau}^{\mathrm{High1}}(\boldsymbol{\eta})$ for the Fast Fading Model

We first write the derivatives of the correlation matrix (14) with respect to the unknown parameters

$$\frac{\partial\mathbf{R}_\mathbf{y}(\boldsymbol{\theta})}{\partial\tau} = \frac{\partial}{\partial\tau}\left(\mathbf{S}\mathbf{R}_\mathbf{f}\mathbf{S}^H + \sigma_n^2\mathbf{I}\right) = \mathbf{S}_\tau\mathbf{R}_\mathbf{f}\mathbf{S}^H + \mathbf{S}\mathbf{R}_\mathbf{f}\mathbf{S}_\tau^H$$
$$\frac{\partial\mathbf{R}_\mathbf{y}(\boldsymbol{\theta})}{\partial\sigma_n^2} = \frac{\partial}{\partial\sigma_n^2}\left(\mathbf{S}\mathbf{R}_\mathbf{f}\mathbf{S}^H + \sigma_n^2\mathbf{I}\right) = \mathbf{I}$$
$$\frac{\partial\mathbf{R}_\mathbf{y}(\boldsymbol{\theta})}{\partial\sigma_f^2} = \frac{\partial}{\partial\sigma_f^2}\left(\mathbf{S}\mathbf{R}_\mathbf{f}\mathbf{S}^H + \sigma_n^2\mathbf{I}\right) = \frac{1}{\sigma_f^2}\mathbf{S}\mathbf{R}_\mathbf{f}\mathbf{S}^H$$
$$\frac{\partial\mathbf{R}_\mathbf{y}(\boldsymbol{\theta})}{\partial\alpha} = \frac{\partial}{\partial\alpha}\left(\mathbf{S}\mathbf{R}_\mathbf{f}\mathbf{S}^H + \sigma_n^2\mathbf{I}\right) = \mathbf{S}\mathbf{R}_\mathbf{f}^{(\alpha)}\mathbf{S}^H \tag{C.1}$$

where $\mathbf{S}_\tau \equiv (\partial/\partial\tau)\,\mathbf{S}$, and $\mathbf{R}_\mathbf{f}^{(\alpha)} \equiv (\partial/\partial\alpha)\,\mathbf{R}_\mathbf{f}$.

Now, in Section III-B1, using (30) and (32), we obtained (29) as $J_{\tau\tau}^{\mathrm{High1}} = 2\mathrm{tr}\{\mathbf{A}\mathbf{R}_\mathbf{f}^{-1}\mathbf{A}^H\mathbf{R}_\mathbf{f} + \mathbf{A}^2\}$ with $\mathbf{R}_\mathbf{f}$ and $\mathbf{R}_\mathbf{f}^{-1}$ given by (15) and (16), respectively. Beginning with the first element, we use the definition of $\mathbf{A}$ in (30) to explicitly write $\mathbf{A}\mathbf{R}_\mathbf{f}^{-1}\mathbf{A}^H$ as

$$\mathbf{A}\mathbf{R}_\mathbf{f}^{-1}\mathbf{A}^H = \frac{1}{\sigma_f^2(1-\alpha^2)}$$
$$\times\begin{bmatrix} a_0a_0^* & -\alpha a_0a_1^* & 0 & 0 & \cdots & 0 \\ -\alpha a_1a_0^* & (1+\alpha^2)a_1a_1^* & -\alpha a_1a_2^* & 0 & & 0 \\ \vdots & & \ddots & \ddots & \ddots & \vdots \\ 0 & 0 & 0 & & & -\alpha a_{N-2}a_{N-1}^* \\ 0 & 0 & 0 & 0 & \cdots & a_{N-1}a_{N-1}^* \end{bmatrix}.$$

The next step is to multiply this matrix with $\mathbf{R_f}$. Since we perform the trace operation on the resulting matrix, we will calculate only the diagonal elements of $\mathbf{A}\mathbf{R}_\mathbf{f}^{-1}\mathbf{A}^H\mathbf{R_f}$

$$\begin{aligned}\text{diag}\left(\mathbf{A}\mathbf{R}_\mathbf{f}^{-1}\mathbf{A}^H\mathbf{R_f}\right) &= \frac{1}{1-\alpha^2} \\ &\times \left[a_0(a_0^* - \alpha^2 a_1^*),\, a_1\left(a_1^* + \alpha^2(a_1^* - a_0^* - a_2^*)\right), \ldots\right. \\ &\quad a_{N-2}\left(a_{N-2}^* + \alpha^2(a_{N-2}^* - a_{N-3}^* - a_{N-1}^*)\right) \\ &\quad \left. a_{N-1}(a_{N-1}^* - \alpha^2 a_{N-2}^*)\right]\end{aligned}$$

where diag$(\cdot)$ denotes "the diagonal elements of $(\cdot)$." The final step is to sum these elements with those of (32) resulting in (33)

$$J_{\tau\tau}^{\text{High1}}(\boldsymbol{\eta}) = \frac{2\alpha^2}{1-\alpha^2}\left[\sum_{i=1}^{N-2} a_i(2a_i^* - a_{i-1}^* - a_{i+1}^*) - a_0 a_1^* - a_{N-1}a_{N-2}^* + a_0 a_0^* + a_{N-1}a_{N-1}^*\right].$$

Appendix D
Proof of Property 2 for the Slow Fading Bound

We begin with the $J_{\tau\tau}^{\text{sf}}$ expressed in term of the phase (23), where for ease of notation, we replace $(\partial/\partial\tau)\,\varphi(iT_s - \tau, \boldsymbol{\eta})$ with p_i. The resulting expression is

$$J_{\tau\tau}^{\text{sf}}(\boldsymbol{\eta}) = \frac{2\rho^2}{1+N\rho}\left[N\sum_{i=0}^{N-1}(p_i)^2 - \left(\sum_{i=0}^{N-1} p_i\right)^2\right]. \quad \text{(D.1)}$$

Examining this expression, we conclude that in order to prove the property, it is enough to show that

$$Z_N \triangleq \frac{1}{1+N\rho}\left(N\sum_{i=0}^{N-1}(p_i)^2 - \left(\sum_{i=0}^{N-1} p_i\right)^2\right)$$

is a nondecreasing function of N or, equivalently, $Z_N - Z_{N-1} \geq 0$, $\forall N > 1$.

Begin by writing the difference explicitly

$$\begin{aligned}Z_N - Z_{N-1} &= \frac{1}{1+N\rho}\left(N\sum_{i=0}^{N-1}(p_i)^2 - \left(\sum_{i=0}^{N-1} p_i\right)^2\right) \\ &\quad - \frac{1}{1+(N-1)\rho} \\ &\quad \times \left((N-1)\sum_{i=0}^{N-2}(p_i)^2 - \left(\sum_{i=0}^{N-2} p_i\right)^2\right) \geq 0.\end{aligned}$$

That is

$$\begin{aligned}&\left(N\sum_{i=0}^{N-1}(p_i)^2 - \left(\sum_{i=0}^{N-1} p_i\right)^2\right) \\ &\quad - \left((N-1)\sum_{i=0}^{N-2}(p_i)^2 - \left(\sum_{i=0}^{N-2} p_i\right)^2\right) \\ &\quad - \frac{\rho}{1+N\rho}\left(N\sum_{i=0}^{N-1}(p_i)^2 - \left(\sum_{i=0}^{N-1} p_i\right)^2\right) \geq 0. \quad \text{(D.2)}\end{aligned}$$

The first two elements can be expanded as

$$\begin{aligned}&Np_{N-1}^2 + N\sum_{i=0}^{N-2}(p_i)^2 \\ &\quad - \left[\left(\sum_{i=0}^{N-2} p_i\right)^2 + 2p_{N-1}\times\sum_{i=0}^{N-2} p_i + p_{N-1}^2\right] \\ &\quad - (N-1)\sum_{i=0}^{N-2}(p_i)^2 + \left(\sum_{i=0}^{N-2} p_i\right)^2 \\ &= (N-1)p_{N-1}^2 + \sum_{i=0}^{N-2}(p_i)^2 - 2p_{N-1}\sum_{i=0}^{N-2} p_i \\ &= \sum_{i=0}^{N-2}\left(p_{N-1}^2 - 2p_{N-1}p_i + (p_i)^2\right) \\ &= \sum_{i=0}^{N-2}(p_{N-1} - p_i)^2.\end{aligned}$$

Plugging this back into (D.2), we are now required to prove that

$$(1+N\rho)\sum_{i=0}^{N-2}(p_{N-1} - p_i)^2 - \rho\left(N\sum_{i=0}^{N-1}(p_i)^2 - \left(\sum_{i=0}^{N-1} p_i\right)^2\right) \geq 0.$$

Expanding and then collecting, we get

$$\begin{aligned}&\sum_{i=0}^{N-2}(p_{N-1} - p_i)^2 + N\rho\sum_{i=0}^{N-2}(p_{N-1} - p_i)^2 \\ &\quad - N\rho\sum_{i=0}^{N-1}(p_i)^2 + \rho\left(\sum_{i=0}^{N-1} p_i\right)^2 \\ &= \sum_{i=0}^{N-2}(p_{N-1} - p_i)^2 \\ &\quad + \rho\left[\left(\sum_{i=0}^{N-1} p_i\right)^2 - 2Np_{N-1}\sum_{i=0}^{N-2} p_i \right. \\ &\qquad \left. + N^2(p_{N-1})^2 - 2N(p_{N-1})^2\right] \\ &= \sum_{i=0}^{N-2}(p_{N-1} - p_i)^2 + \rho\left(\left(\sum_{i=0}^{N-1} p_i\right) - Np_{N-1}\right)^2.\end{aligned}$$

The last expression is obviously non-negative, implying that increasing the number of samples does not decrease the $J_{\tau\tau}^{\text{sf}}$, which proves the property.

REFERENCES

[1] T. S. Rappaport, *Wireless Communications—Principles and Practice*. Englewood Cliffs, NJ: Prentice-Hall, 1996.

[2] U. Mengali and A. D'Andrea, *Synchronization Techniques for Digital Receivers (Application of Communication Theory)*. New York: Plenum, 1997.

[3] U. Mengali, A. N. D'Andrea, and M. Morelli, "Symbol timing estimation with CPM modulation," *IEEE Trans. Commun.*, vol. 44, pp. 1362–1371, Oct. 1996.

[4] T. Aulin and C.-E. Sundberg, "Synchronization properties of continuous phase modulation," in *Proc. Global Telecommun. Conf.*, Miami, FL, Nov. 1982, pp. D7.1.1–D7.1.7.

[5] F. Patenaude, J. H. Lodge, and P. A. Galko, "Symbol timing tracking for continuous phase modulation over fast flat-fading channels," *IEEE Trans. Veh. Technol.*, vol. 40, pp. 615–626, Aug. 1991.

[6] K. Goethals and M. Moeneclaey, "Tracking performance of ML-oriented NDA symbol synchronizers for nonselective fading channels," *IEEE Trans. Commun.*, vol. 43, pp. 1179–1184, Feb./Mar./Apr. 1995.

[7] H. L. Van Trees, *Detection, Estimation, and Modulation Theory—Part III*. New York: Wiley, 1971.

[8] S. S. Soliman and R. A. Scholtz, "Synchronization over fading dispersive channels," *IEEE Trans. Commun.*, vol. 36, pp. 499–505, Apr. 1988.

[9] F. Gini and G. B. Giannakis, "Frequency offset estimation and symbol timing recovery in flat-fading channels: A cyclostationary approach," *IEEE Trans. Commun.*, vol. 46, pp. 400–411, Mar. 1998.

[10] M. Ghogho, A. Swami, and T. Durrani, "On blind carrier recovery in time-selective fading channels," in *Proc. 33rd Asilomar Conf. Signals, Syst., Comput.*, vol. 1, Pacific Grove, Oct. 1999, pp. 243–247.

[11] K. E. Scott and E. B. Olasz, "Simultaneous clock phase and frequency offset estimation," *IEEE Trans. Commun.*, vol. 43, pp. 2263–2270, July 1995.

[12] A. Swami, M. Ghogho, and T. Durrani, "Blind synchronization and Doppler spread estimation for MSK signals in time-selective fading channels," in *Proc. ICASSP*, vol. 5, Istanbul, Turkey, June 2000, pp. 2665–2668.

[13] M. Ghogho and A. Swami, "CRB's and estimators for the parameters of time selective fading channels," in *Proc. SPWAC*, Annapolis, MD, May 1999, pp. 407–410.

[14] F. Gini, M. Luise, and R. Reggiannini, "Cramer–Rao bounds in the parametric estimation of fading radiotransmission channels," *IEEE Trans. Commun.*, vol. 46, pp. 1390–1398, Oct. 1998.

[15] J. M. Francos and B. Friedlander, "Bounds for estimation of multicomponent signals with random amplitude and deterministic phase," *IEEE Trans. Signal Processing*, vol. 43, pp. 1161–1172, May 1995.

[16] T. Aulin and C.-E. W. Sundberg, "Continuous phase modulation—Part I: Full response signaling," *IEEE Trans. Commun.*, vol. COMM-29, pp. 196–209, Mar. 1981.

[17] H. Taub and D. L. Schilling, *Principles of Communication Systems*, 2nd ed. New York: McGraw-Hill, 1986.

[18] W. C. Jakes, *Microwave Mobile Communications*. New York: Wiley, 1974.

[19] M. Moeneclaey, H. Meyr, and S. A. Fechtel, *Digital Communication Receivers: Synchronization, Channel Estimation and Signal Processing*. New York: Wiley, 1997.

[20] O. Besson, F. Vincent, P. Stoica, and A. B. Gershman, "Approximate maximum likelihood estimators for array processing in multiplicative noise environments," *IEEE Trans. Signal Processing*, vol. 48, pp. 2506–2518, Sept. 2000.

[21] C. B. Chang and R. W. Miller, "A modified Cramer–Rao bound and its applications," *IEEE Trans. Inform. Theory*, vol. IT-24, pp. 398–400, May 1978.

[22] S. M. Kay, *Fundamentals of Statistical Signal Processing: Estimation Theory*. Englewood Cliffs, NJ: Prentice-Hall, 1993.

[23] P. Stoica and A. Nehorai, "Performance study of conditional and unconditional direction-of-arrival estimation," *IEEE Trans. Acoust., Speech, Signal Processing*, vol. 38, pp. 1783–1795, Oct. 1990.

[24] J. Goldberg, G. Fuks, and H. Messer, "Bearing estimation in a Ricean channel—Part I: Inherent accuracy limitations," *IEEE Trans. Signal Processing*, vol. 49, pp. 925–937, May 2001.

Ron Dabora was born in Tel Aviv, Israel, in 1972. He received the B.Sc. and M.Sc. degrees, both with high distinction, in electrical engineering from Tel Aviv University in 1994 and 2000, respectively.

Since 2000, he has been with Millimetrix Broadband Networks, Israel, where he is a member of the Algorithms Development Group.

Jason Goldberg (SM'99) was born in New Haven, CT, in 1965. He received the B.S.E.E. (with high distinction) and Ph.D. degrees in electrical engineering from Worcester Polytechnic Institute, Worcester, MA, and the University of London, London, U.K., in 1988 and 1993, respectively.

From 1993 to 1996, he was a Postdoctoral Researcher at Polytechnic University of Catalonia, Barcelona, Spain. Since 1996, he has been a researcher at Tel Aviv University, Tel Aviv, Israel, in the area of statistical and array signal processing. In 1998, he also joined the Research Group at the Cellular Communications Division of Intel, Petach Tikva, Israel, where he works on the design and analysis of algorithms for wireless communications.

Hagit Messer (F'00) received the B.Sc, M.Sc., and Ph.D. degrees in electrical engineering from Tel Aviv University, Tel Aviv, Israel, in 1977, 1979, and 1984, respectively.

Since 1977, she has been with the Department of Electrical Engineering—Systems at the Faculty of Engineering, Tel Aviv University, first as a Research and Teaching Assistant and then, after a one-year post-doctoral appointment at Yale University (from 1985 to 1986), as a Faculty Member. Her research interests are in the field of signal processing and statistical signal analysis. Her main research projects are related to tempo-spatial and non-Gaussian signal detection and parameter estimation.

Dr. Messer was an Associate Editor for the IEEE TRANSACTIONS ON SIGNAL PROCESSING from 1994 to 1996, and she is now an Associate Editor for the IEEE SIGNAL PROCESSING LETTERS. She is a Member of the Technical Committee of the IEEE Signal Processing Society for Signal Processing, Theory, and Methods and a co-organizer of the IEEE workshop HOS'99. Since 2000, she has been the Chief Scientist of the Israeli Ministry of Science, Culture, and Sport.